

A risk-scoring model based on endobronchial ultrasound multimodal imaging for predicting metastatic lymph nodes in lung cancer patients

Zhihong Huang^{1,2,3}, Lei Wang⁴, Junxiang Chen^{1,2,3}, Xinxin Zhi^{1,2,3}, Jiayuan Sun^{1,2,3,*}

ABSTRACT

Background and Objectives: Endobronchial ultrasound (EBUS) imaging is a valuable tool for predicting lymph node (LN) metastasis in lung cancer patients. This study aimed to develop a risk-scoring model based on EBUS multimodal imaging (grayscale, Doppler mode, elastography) to predict LN metastasis in lung cancer patients.

Patients and Methods: This retrospective study analyzed 350 metastatic LNs in 314 patients with lung cancer and 124 reactive LNs in 96 patients with nonspecific inflammation. The sonographic findings were compared with the final pathology results and clinical follow-up. Univariate and multivariate logistic regression analyses were performed to evaluate the independent risk factors of metastatic LNs. According to the β coefficients of corresponding indicators in logistic regression analysis, a risk-scoring model was established. Receiver operating characteristic curve was applied to evaluate the predictive capability of model.

Results: Multivariate analysis showed that short axis >10 mm, distinct margin, absence of central hilar structure, presence of necrosis, nonhilar vascularity, and elastography score 4 to 5 were independent predictors of metastatic LNs. Both short axis and margin were scored 1 point, and the rest of independent predictors were scored 2 points. The combination of 3 EBUS modes had the highest area under the receiver operating characteristic and accuracy of 0.884 (95% confidence interval, 0.846–0.922) and 87.55%, respectively. The risk stratification was as follows: 0 to 2 points, malignancy rate of 11.11%, low suspicion; 3 to 10 points, malignancy rate of 86.77%, high suspicion.

Conclusions: The risk-scoring model based on EBUS multimodal imaging can effectively evaluate metastatic LNs in lung cancer patients to support clinical decision making.

Keywords: Endobronchial ultrasound; Multimodal imaging; Lung cancer; Lymph nodes; Risk stratification

INTRODUCTION

Lung cancer is the leading cause of cancer-related mortality worldwide.^[1,2] Correctly staging lung cancer is of great importance because the treatment strategies and outcomes differ significantly by stage.^[3,4] Endobronchial ultrasound-guided transbronchial aspiration (EBUS-TBNA) is recommended as a first-line investigation for intrathoracic nodal staging in lung cancer owing to its minimally invasive nature and high sensitivity.^[5] However, EBUS-TBNA has an average false-negative rate of 24% (ranging from 1% to 37%) in lung

cancer patients.^[6] The false-negative EBUS-TBNA findings are caused by inadequate specimens in the lymph nodes (LNs).^[7] This indicates that proper interpretation of EBUS imaging and a suitable choice of target LNs are essential to increase the diagnostic rate and reduce false negatives.

EBUS imaging can reflect the characteristics of LNs, and it has been demonstrated in several studies that certain EBUS features can be used to distinguish between benign and malignant intrathoracic LNs during EBUS-TBNA.^[8–10] However, ultrasonic characteristics of LNs are different between various malignant diseases, which may affect the judgment to predict metastatic LNs.^[11] Previous studies have individually demonstrated that grayscale feature, Doppler mode, and elastography may assist clinicians to predict LN metastasis during EBUS-TBNA.^[12–16] To our knowledge, there is still a lack of research on a combination of 3 EBUS modes.

This study aimed to construct a risk-scoring model to predict metastatic intrathoracic LNs in lung cancer patients based on EBUS multimodal imaging. Furthermore, a risk stratification method is proposed to facilitate clinical decision making in the background of nondiagnostic EBUS-TBNA.

MATERIALS AND METHODS

Patients and LNs

This retrospective study was approved by the Ethics Committee of Shanghai Chest Hospital (KS1946). The need for informed consent was waived because of the retrospective nature of the study.

¹Department of Respiratory Endoscopy, Shanghai Chest Hospital, Shanghai Jiao Tong University School of Medicine, Shanghai 200030, China; ²Department of Respiratory and Critical Care Medicine, Shanghai Chest Hospital, Shanghai Jiao Tong University School of Medicine, Shanghai 200030, China; ³Shanghai Engineering Research Center of Respiratory Endoscopy, Shanghai 200030, China; ⁴Department of Ultrasound, Shanghai Chest Hospital, Shanghai Jiao Tong University School of Medicine, Shanghai 200030, China.

* **Address for correspondence:** Department of Respiratory Endoscopy, Department of Respiratory and Critical Care Medicine, Shanghai Chest Hospital, Shanghai Jiao Tong University School of Medicine, 241 West Huaihai Road, Shanghai 200030, China. E-mail: xkyjysun@163.com. (J Sun).

Copyright © 2024 The Author(s). Published by Wolters Kluwer Health, Inc on behalf of Scholar Media Publishing. This is an open access article distributed under the Creative Commons Attribution-NonCommercial-ShareAlike License 4.0 (CC BY-NC-SA) which allows others to remix, tweak, and build upon the work non-commercially, as long as the author is credited and the new creations are licensed under the identical terms.

Endoscopic Ultrasound (2024) 13:2

Received: 5 June 2023; Accepted: 9 November 2023

Published online: 1 February 2024

<http://dx.doi.org/10.1097/eus.0000000000000051>

Consecutive patients with intrathoracic lymphadenopathy who underwent EBUS-TBNA with multimodal videos (grayscale, Doppler, and elastography) in our hospital from September 2019 to June 2020 were analyzed. EBUS-TBNA was performed in patients meeting the following criteria: (1) enlarged mediastinal/hilar LNs (at least 1 node >1 cm in the short axis) based on computed tomography (CT) or positive intrathoracic LNs/lesions detected (defined as standardized uptake value >2.5) by positron emission tomography-computed tomography (PET/CT); (2) pathological confirmation was clinically required, and EBUS-TBNA examination was feasible; and (3) no contraindication to the procedure. All patients signed an informed consent form for EBUS-TBNA examination. Patients who were confirmed with lung cancer or nonspecific inflammation by pathology and clinical follow-up were finally included in this study. The flowchart of patients and LNs is shown in Figure 1.

LN stations were defined by the TNM classification.^[17] The diagnosis of metastatic LNs was based on the malignant cytologic or histologic results of EBUS-TBNA or on surgical-pathologic confirmation. The diagnosis of reactive LNs was established when pathologic findings demonstrated lymphocytes or inflammatory cells, and LN size was stable or diminished with antibiotic treatment during the follow-up. EBUS-TBNA samples were classified as “true-positive” if malignant cells were found and “true-negative” if nonmalignant diagnoses were confirmed at a clinical follow-up (eg, further tests and CT).^[18] To avoid false-negative results of EBUS-TBNA, reactive LNs were only selected from patients with nonspecific inflammation and with at least 24 months of clinical follow-up.^[14]

Measurement of CT and PET/CT parameters

The measurement of CT and PET/CT was performed according to a one-to-one correlation between CT or PET/CT images of LNs and the EBUS-TBNA region by the same groups of LNs. Short diameter was measured at the maximum cross section of the target LN on the mediastinal window settings (window width, 350 Hounsfield unit; window level, 50 Hounsfield unit). The short diameter >10 mm on axial CT was suspected malignancy. The maximum standardized

uptake value (SUVmax) was obtained by drawing regions of interest on attenuation-corrected fluorodeoxyglucose-PET fusion images around the involved LN group.^[19] SUVmax >2.5 was used to predict malignant LNs. The time interval between CT or PET/CT and EBUS-TBNA was less than 1 month.

EBUS-TBNA procedure

The targeted LNs and peripheral vessels were examined using a convex probe ultrasound bronchoscopy (BF-UC260FW; Olympus, Tokyo, Japan) with the scanning frequency of 10 MHz. The grayscale features, vascular patterns, and elastography were recorded by ultrasound processor (EU-ME2; Olympus). A grayscale image was frozen at the maximal cross sections to measure the diameter of targeted LN. To guarantee optimum sensitivity and prevent artifactual color noise caused by the breathing and heartbeats, color gain was increased until background noise arose, and then lowered until the noise was controlled.^[14] Before observing EBUS elastography, the region of interest was set to include the targeted LN and peripheral tissue except the vessels. The satisfactory EBUS elastography was usually generated by internal compression from the heart and blood vessel movement. If the image is not ideal, an up-down angle lever of the bronchoscope will be used at a frequency of 3 to 5 times per second.^[15,20] After the operation, bronchoscopists saved the following videos: a 10-second grayscale video, a 20-second blood flow Doppler video, and two 20-second elastography videos.

Finally, operators used a 22-gauge needle to puncture the targeted LN under the guidance of real-time EBUS. Three needle aspirations were recommended for each LN. If an obvious histology specimen was obtained, however, 2 aspirations were acceptable. Rapid on-site evaluation was not performed for all LNs.

EBUS image features of LNs

EBUS modes were categorized as grayscale mode, Doppler mode, and elastography mode. The representative sonographic features corresponding EBUS modes are shown in Figure 2. Grayscale features included short axis (>10 or ≤10 mm), shape (round or oval), margin (distinct or indistinct), echogenicity (heterogeneous or homogeneous), central hilar structure (CHS; present or absent), necrosis (present or absent), matting (present or absent), and calcification (present or absent).^[14,21] The long axis was the maximum diameter of the largest section of the LN in grayscale images, and the short axis was the largest diameter perpendicular to the long axis. When the ratio of the long axis and short axis was greater than 1.5, it was defined as oval. When more than half of the margin (the boundary between the LN and surrounding soft tissues) was clearly visualized with a high echoic border, it was defined as a distinct margin. Echogenicity of the LNs is considered heterogeneous if the echoes show a nonuniform pattern. When a continuous linear and hyperechoic region was found in the center of the LN, CHS was considered present. Necrosis sign is an abnormal echoic area within the LN without blood flow, and it may appear as an anechoic area (cystic necrosis) or an echogenic area (coagulation necrosis). The nodes were considered matted when the LNs were in confluence and no normal soft tissues intervened between them. Calcification was commonly characterized by a hyperechoic structure of various shapes with an acoustic shadow.

Vascular distribution patterns were evaluated using Doppler mode^[14]: (1) avascular, the absence of vascular signals within the LNs; (2) hilar, flow of signal that branches radially from the hilus, regardless of whether the signals originated from the central region or from the eccentric; and (3) nonhilar, which includes central, capsular, and

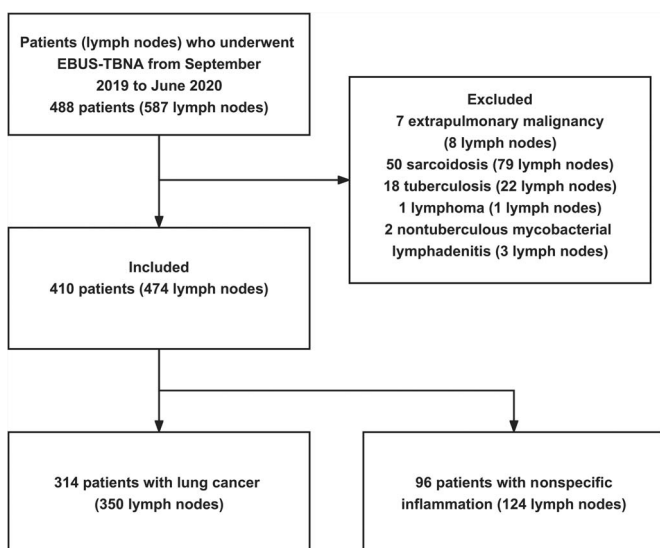


Figure 1. Flow diagram of patient and lymph node enrollment. EBUS-TBNA: endobronchial ultrasound-guided transbronchial needle aspiration.

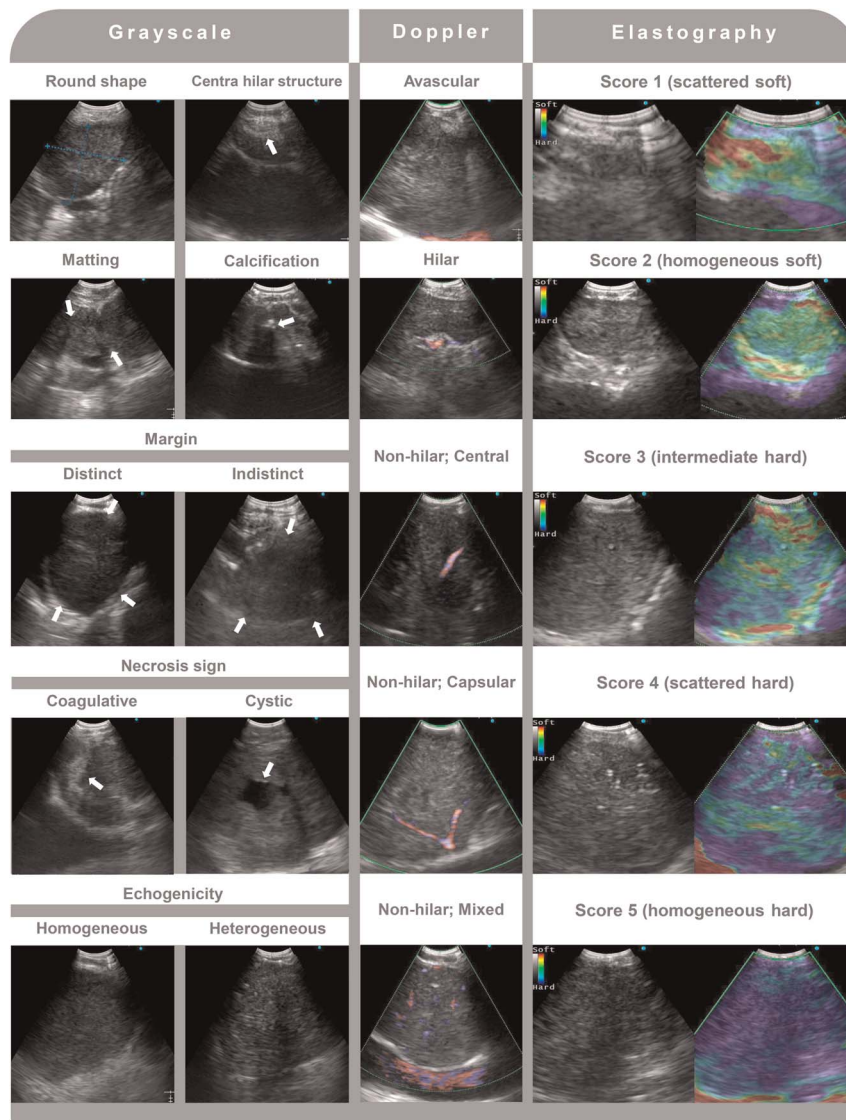


Figure 2. Representative sonographic features used for classifying metastatic and reactive lymph nodes.

mixed (≥ 2 types mixed from the hilar, central, and capsular). Central pattern appears as a scattering of patches or segments of vascular signal within the node (deformed radial, aberrant multifocal). Capsular (or peripheral) pattern is characterized by the flow of signals along the LNs' periphery with branches penetrating the node's periphery and not originating from the hilar arteries.

In elastography mode, a qualitative 5-score method was used to identify the hardness of LNs^[15]: score 1 represents a heterogeneous soft pattern (mixed green-yellow-red), score 2 represents a homogeneous soft pattern (predominantly green), score 3 represents an intermediate hardness pattern (mixed blue-green-yellow-red), score 4 represents a heterogeneous hard pattern (mixed blue-green), and score 5 represents a homogeneous hard pattern (predominantly blue).

The following manifestations were considered metastatic LNs based on our previous studies^[14,15,20]: short axis >10 mm, round shape, distinct margin, heterogeneity, absence of CHS, presence of necrosis,

presence of matting, presence of calcification, nonhilar vascularity, and elastography score of 4 to 5. These sonographic features, CT short diameter, and SUVmax on PET/CT were compared with the final pathology outcomes to calculate the diagnostic accuracies.

Intraobserver and interobserver agreement of EBUS image features

In this study, 3 experienced doctors independently evaluated the aforementioned sonographic features twice independently blind to the final diagnosis of the LNs and the clinical data of patients, and then intraobserver agreement was calculated. To determine the interobserver agreement among the 3 doctors, each doctor provided a final value for the different outcomes of the 2 assessments. The 3 doctors' divergent opinions were discussed together to reach a consensus that was then applied to subsequent analysis. κ Values ranging from 0.81 to 1.00 were considered as almost perfect; 0.61 to 0.80, substantial; 0.41 to 0.60, moderate; 0.21 to 0.40, fair; and 0.00 to 0.20, slight agreement.^[22]

Table 1
Characteristics of patients and lymph nodes

Characteristics	Cases
Patients, <i>n</i>	410
Sex (male/female)	304/106
Age, median (range), <i>y</i>	64 (23–84)
Diagnosis of patients, <i>n</i> (%)	
Lung cancer	314 (76.59)
Adenocarcinoma	137 (33.41)
Squamous carcinoma	45 (10.98)
Small cell lung cancer	81 (19.76)
Others	51 (12.43)
Nonspecific inflammation	96 (23.41)
Lymph nodes, <i>n</i>	474
Long axis on EBUS, mm	21.36 ± 7.52
Short axis on EBUS, mm	16.80 ± 6.87
Short diameter on CT, mm	16.61 ± 7.43
SUVmax on PET, <i>n</i> (%)	
>2.5	121 (25.53)
≤2.5	6 (1.26)
Not evaluated	347 (73.21)
Diagnosis of lymph nodes, <i>n</i> (%)	
Metastatic lymph nodes	350 (73.84)
Reactive lymph nodes	124 (26.16)
Station, <i>n</i> (%)	
2R, 4R, 4 L	190 (40.08)
7	163 (34.39)
10R, 10 L	13 (2.74)
11 L, 11Rs, 11Ri	108 (22.78)

EBUS: endobronchial ultrasound; CT: computed tomography; PET: positron emission tomography; SUVmax: maximum standardized uptake value.

Statistical analysis

All features were classified into 2 categories. Cohen κ method was used to analyze intraobserver and interobserver agreement. The χ^2 test or Fisher exact test by univariate analysis was used for each sonographic feature. The features selected by univariate analysis were then further assessed using the binary logistic regression method, and the risk score of each feature was determined according to the β coefficients obtained from the logistic regression method.^[23] The largest β coefficient (β_{max}) was selected to establish the highest score of the feature. The points of each feature were calculated by $Points = 2\beta/\beta_{max}$, and the points were rounded to the nearest integer.

A receiver operating characteristic (ROC) curve and the area under the ROC curve (AUC) were performed to identify predictive capability of model. DeLong test was used to compare the 2 ROC curves. For missing data, we performed statistical analysis based on pairwise deletion method.^[24] The sensitivity, specificity, positive predictive value, negative predictive value, and diagnostic accuracy rate were calculated according to standard definitions. To perform internal validation of the risk-scoring model, 1000 bootstrap samples from the original sample were used.^[25] Hosmer-Lemeshow test was used to evaluate the model’s predictive accuracy. All statistical tests were 2-sided. A *P* value of less than 0.05 was deemed statistically significant. The statistical analyses were performed with R (version 4.0.4; R Foundation for Statistical Computing) and STATA 16 (Stata Corp, College Station, TX).

Results

Patients and LNs

Four hundred ten patients were eligible and analyzed in this study. Of them, 314 were diagnosed with lung cancer, and 96 had nonspecific inflammation. The pathology types of lung cancer were adenocarcinoma in 137, squamous carcinoma in 45, small cell lung cancer in 81, and others in 51 (5 pulmonary sarcomatoid carcinoma, 22 non-small cell lung cancer, 9 neuroendocrine tumor, and 15 unknown type of lung cancer). The median age was 64 (range, 23–84) years. A total of 474 LNs from 410 patients were analyzed, including 350 metastatic LNs and 124 reactive LNs. The largest proportion of biopsied stations was 7 (34.39%), followed by 4R (30.38%) and 11L (8.44%). The characteristics of the patients and LNs are illustrated in Table 1. Chest CT results were not available for 11 patients with 12 LNs because they underwent CT examinations at other hospitals. The short diameter on CT was 379 LNs >10 mm and 83 LNs ≤10 mm. The mean short diameter on CT was 16.61 ± 7.43 mm. PET/CT results were evaluated for 127 LNs (26.79%), among which 121 LNs (25.53%) had SUVmax >2.5. A pairwise deletion method was performed to handle the missing data for CT and PET/CT.

Relationship between sonographic features and metastatic LNs

All features, except necrosis, had a perfect intraobserver and interobserver agreement [Table 2]. In univariate analysis, all sonographic features, except calcification, were considered significant predictors of metastatic LNs with *P* < 0.05 [Table 3]. These predictors were included in the multivariate logistic regression analysis. The results of multivariate analysis are shown in Table 4. The following 6 features were independent predictors of metastatic LNs (*P* < 0.05): short axis >10 mm, distinct margin, absence of CHS, presence of necrosis, nonhilar vascular pattern, and elastography score 4 to 5. According to β acquired from multivariate analysis, both short axis and margin were scored 1 point, and the rest of independent predictors were scored 2 points.

Construction and validation of a risk-scoring model

The ROC curves of different EBUS modalities were established based on the aforementioned points of corresponding features. The ROC curves of all modalities are shown in Figure 3. The diagnostic performance for each mode, as well as for combinations of different EBUS modes, is provided in Table 5. Cutoff values of each modality were determined by the points with the highest accuracy. The grayscale features combined with vascularity distribution and elasticity showed

Table 2
Intraobserver and interobserver agreement of sonographic features

Sonographic Features	κ	
	Intraobserver Agreement	Interobserver Agreement
Margin	0.959	0.808
Echogenicity	0.965	0.835
CHS	0.957	0.881
Necrosis	0.895	0.778
Matting	0.924	0.885
Calcification	0.980	0.883
Hilar vascularity	0.932	0.849
Elastography	0.956	0.917

CHS: central hilar structure.

Table 3
Univariate analysis of sonographic features for predicting metastatic lymph nodes

Sonographic Features	SE, %	SP, %	PPV, %	NPV, %	ACC, %	P
Short axis >10 mm	77.89	47.37	88.57	29.03	73.00	<0.001
Round shape	76.29	33.87	76.50	33.60	65.19	0.027
Distinct margin	76.86	33.87	76.64	34.15	65.61	0.019
Heterogeneity	72.00	65.32	85.42	45.25	70.25	<0.001
Absence of CHS	89.43	70.16	89.43	70.16	84.39	<0.001
Presence of necrosis	31.14	95.97	95.61	33.06	48.10	<0.001
Presence of matting	26.57	95.97	94.90	31.65	44.73	<0.001
Calcification	15.43	88.71	79.41	27.09	34.60	0.259
Nonhilar vascularity	89.71	71.77	89.97	71.20	85.02	<0.001
Elastography 4–5	80.29	70.16	88.36	55.77	77.64	<0.001

ACC: accuracy; CHS: central hilar structure; NPV: negative predictive value; PPV: positive predictive value; SE: sensitivity; SP: specificity.

good predictive accuracy with the highest AUC of 0.884 (95% confidence interval, 0.846–0.922) and accuracy of 87.55%. Meanwhile, the sensitivity, specificity, positive predict value, and negative predict value were 96.57%, 62.10%, 87.79%, and 86.52%, respectively. Then, the risk-scoring model was produced from the combination of 3 EBUS modes, which significantly outperformed CT short diameter and SUVmax parameters (Delong test, both $P < 0.001$).

The malignant rate ranged from 0% to 100% in the order of calculated risk scores [Table 6], and then the total score was divided into 2 groups depending on malignancy rate [Table 7]: 0 to 2 points, with the malignancy rate of 11.11%, related to low suspicion; 3 to 10 points, with the malignancy rate of 86.77%, related to high suspicion. For internal validation, the risk-scoring model indicated good fit using Hosmer-Lemeshow test with $P = 0.665$. The corrected AUC (0.885) was also high in bootstrap validation.

DISCUSSION

The evaluation of intrathoracic LNs is a crucial procedure for lung cancer patients because it involves the prognosis of patients and choice of treatment. Ultrasonographic features were suggested to predict benign or malignant LNs in patients undergoing EBUS-TBNA.^[26] As the elastography mode has been developed, it can be used with grayscale and Doppler mode, which makes the predictions more accurate. In this study, a risk-scoring model was constructed by 3 EBUS modes (grayscale, Doppler mode, and elasticity) and had the highest AUC value as well as the highest accuracy. For clinical practice, the risk stratification of our model was categorized as low and high suspicion according to the malignant rate.

This study revealed that short axis >10 mm, distinct margin, presence of necrosis, absence of CHS, nonhilar vascularity, and elastography of

score 4 to 5 were independent risk factors on EBUS. For size, a short axis of >10 mm was considered as an independent risk predictor, consistent with most studies.^[20,21,27] An increase in nodal size may suggest metastatic involvement in patients with a known primary lung cancer. However, reactive LNs can be as large as metastatic LNs, whereas malignancy can be found in small nodes.^[28] Hence, it could not be used as an absolute criterion. For margin, distinct border seen in malignant nodes may result from nodal infiltration by tumor cells replacing the normal tissue, which caused an increased difference in acoustic impedance.^[29] In our previous study, sarcoid nodes had distinct borders (97.9%),^[30] so sarcoid nodes should be excluded to avoid affecting the judgment of the difference between metastatic and reactive LNs. Necrosis was caused by excessive tumor growth and insufficient blood supply.^[29] However, it was often seen in tuberculous nodes (83.8%),^[30] which were also excluded. The absence of CHS had the highest sensitivity of 89.43% and diagnostic accuracy of 84.39% in grayscale features. Metastatic LNs usually tend to manifest as no hilum or eccentric hilum caused by infiltration and compression of tumor tissue or necrotic tissue.^[21] Lin et al.^[31] found that CHS might still be preserved in the early stage of metastasis. A systematic review included 29 articles and found that the absence of CHS was seen by 16 studies and had the highest pooled sensitivity of 0.91 (95% confidence interval, 0.90–0.92).^[29]

For Doppler mode, our results showed that vascularity distribution had the highest accuracy of 85.02% in all sonographic features. Other studies that used blood flow grade instead of vascular distribution to predict metastasis found that it was not significant independent predictors of LNs metastasis.^[21,32] This reason might be that blood flow grade was more affected by external factors, such as pulsation of great vessels and respiratory movement.^[14] The elastography had the accuracy of 77.64%, which was a useful EBUS modality to detect the tissue stiffness.^[16,33] However, previous studies also found that some

Table 4
β Coefficients for the selected sonographic features by multivariate analysis and corresponding weighting

Variable	P	β Coefficients	OR	95% Confidence Interval	Allocated Score
Short axis >10 mm	0.016	0.89	2.433	1.181–5.014	1
Distinct margin	0.003	1.00	2.706	1.412–5.188	1
Absence of CHS	0.003	1.25	3.484	1.525–7.959	2
Presence of necrosis	0.014	1.28	3.604	1.291–10.061	2
Nonhilar vascularity	<0.001	1.59	4.884	2.129–11.204	2
Elastography 4–5	<0.001	1.20	3.314	1.829–6.002	2

CHS: central hilar structure; OR: odd ratio.

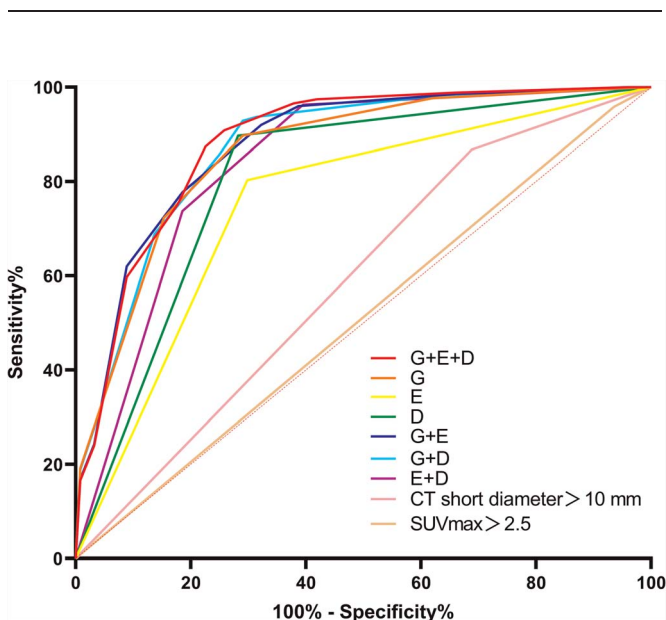


Figure 3. Receiver operating characteristic curves of different predictive models for predicting metastatic lymph nodes in lung cancer. A combination of 3 EBUS modes (G + E + D), 2-combined-mode model (G + E, G + D, and E + D). D: Doppler mode; E, elastography; EBUS: endobronchial ultrasound; G: grayscale feature.

false-positive cases might be caused by patients with nonspecific inflammation, which had areas of hard fibrotic or anthracotic tissues.^[15] To sum up, each sonographic feature had 2 sides and should not be the sole criterion in assessment of intrathoracic LNs in lung cancer, so a combination of each feature was suggested.

Comparing with a single EBUS mode, the combination of multiple EBUS modes not only obtained higher accuracy but also reflected more comprehensive characteristics of LNs. In addition, different sonographic features of LNs have different β value, which implies the different weight of malignancy. Hylton and associates^[27] developed the Canada LN score based on the weighting of different risk predictors and showed satisfactory capability of predicting malignant LNs (AUC, 0.719), but their model just used grayscale features alone. Morishita et al.^[32] found that their model, 4 grayscale features combining with elastography mode, had a higher AUC value than the Canada LN score (AUC, 0.894 vs. 0.756; $P < 0.001$). Zhi et al.^[20]

Table 6

Predictive total scores and malignancy rates of lymph nodes based on the risk-scoring model

Score	No. Malignant (n = 350)	No. LNs (n = 474)	Malignancy Rate, %
0	0	5	0.00
1	4	41	9.76
2	5	35	14.29
3	3	8	37.50
4	20	35	57.14
5	12	16	75.00
6	43	49	87.76
7	54	65	83.08
8	125	132	94.70
9	26	29	89.66
10	58	59	98.31

LNs: lymph nodes.

included all patients who underwent EBUS-TBNA and found that grayscale combining with elastography had the best performance, and the accuracy in validation group was 84.1% when at least 2 of the 3 features (absence of CHS, heterogeneity, and qualitative elastography score 4–5). Schmid-Bindert and associates^[34] established a sum score prediction model for malignancy based on 6 EBUS features (short axis, echogenicity, shape, margin, CHS, and blood flow), and found that LN was considered as high risk of malignancy if more than 2 positive EBUS features were present. There were 2 differences between these studies and ours as follows: on the one hand, these studies used the calculating number of EBUS features to establish a predictive model, which ignored the risk weight of each EBUS features; on the other hand, they included various types of LNs rather than metastatic LNs of lung cancer and reactive LNs, which may affect the diagnostic accuracy of model for predicting metastatic LNs in lung cancer.

In this study, according to β value obtained by logistic regression analysis, we assigned weights to statistically significant features instead of arbitrary weights, which could reflect the risk of different features more accurately. Among any combination of 3 EBUS modes, the 3 combined models obtained the highest AUC value of 0.884 and then was used to construct the risk-scoring model for clinical application. For internal validation, we corroborated the validation with 1000 samples and obtained a satisfactory corrected AUC value of 0.885, which indicated that this model has good stability. This model outperformed any single EBUS mode as well as the combination of

Table 5

Diagnostic performances of different predictive models and their corresponding cutoff values

Model	Cutoff	SE, %	SP, %	PPV, %	NPV, %	ACC, %	AUC (95% CI)	Compared With G + D + E Model
G + D + E	≥4	96.57	62.10	87.79	86.52	87.55	0.884 (0.846–0.922)	—
G	≥3	89.71	70.97	89.71	70.97	84.81	0.863 (0.824–0.901)	$P = 0.041$
D	≥2	89.71	71.77	89.97	71.20	85.02	0.807 (0.765–0.850)	$P < 0.001$
E	≥2	80.29	70.16	88.36	55.77	77.64	0.752 (0.707–0.798)	$P < 0.001$
G + D	≥3	93.71	68.55	89.37	79.44	87.13	0.873 (0.835–0.911)	$P = 0.178$
G + E	≥3	96.00	61.29	87.50	84.44	86.92	0.877 (0.840–0.915)	$P = 0.111$
E + D	≥2	96.29	60.48	87.31	85.23	86.92	0.840 (0.797–0.833)	$P < 0.001$
CT short diameter >10 mm	≥1	86.76	31.15	77.84	45.78	72.08	0.590 (0.545–0.635)	$P < 0.001$
SUVmax >2.5	≥1	95.83	6.45	76.03	33.33	74.02	0.511 (0.463–0.560)	$P < 0.001$

ACC: accuracy; AUC: areas under curve; CI: confidence interval; CT: computed tomography; D: Doppler mode; E: elastography mode; G: grayscale feature (short axis >10 mm, distinct margin, presence of necrosis, and absence of central hilar structure); PET: positron emission tomography; NPV: negative predictive value; PPV: positive predictive value; SE: sensitivity; SP: specificity; SUVmax: maximum standardized uptake value.

Table 7
Risk stratification based on the risk-scoring model

Score	Total (n = 474)			Risk Stratification
	No. Malignant	No. LNs	Malignancy Rate, %	
0–2	9	81	11.11	Low suspicion
≥3	341	393	86.77	High suspicion

EBUS-TBNA: endobronchial ultrasound–guided transbronchial needle aspiration; LNs: lymph nodes.

elasticity and vascularity distribution (all $P < 0.05$). The differences between the 3-combined-mode model and the rest of 2-combined-mode model were not statistically significant. Our results showed that 36 metastatic LNs (10.3%) were considered as benign by using the vascularity distribution, whereas 26 of them were considered as malignant by using the elasticity. Adversely, 37 reactive LNs (29.8%) were deemed as malignant by the elasticity, whereas 14 of them were deemed as benign by using the vascularity distribution. This implied that elasticity and vascularity distribution might be mutually complementary. Therefore, it was essential to diagnose metastatic LNs in lung cancer by using EBUS multimodal imaging. In addition, the cutoff of 3-combined-mode model also had the highest accuracy of 87.55%.

The most used CT-based diagnostic criterion for intrathoracic LNs is a maximal short diameter >10 mm.^[35] In this study, the sensitivity and specificity of the size criteria were 86.76% and 31.15%, respectively, similar to a previous study.^[19] The number of PET/CT performed on reactive LNs was only 31, of which 29 LNs were diagnosed as malignant based on SUVmax >2.5 ; thus, the specificity of SUVmax was low at 6.45%, but the sensitivity was 95.83%. Compared with CT and PET/CT, our EBUS multimodal imaging had a higher diagnostic accuracy. Nevertheless, the diagnostic performance of CT or PET/CT should be reflected by a variety of parameters but not only CT short diameter or SUVmax. A further multimodal medical image study should be performed to address this problem.

For the convenience of clinical applications, we classified the risk-scoring model based on the distribution of the total score and the malignancy rate. The following suggestions were given. For 0 to 2 points, according to the total malignancy rate of 11.11%, it was classified as low suspicious malignancy. The follow-up was recommended first instead of the further invasive methods when the pathology of EBUS-TBNA was negative with qualified specimens. For 3 to 4 points, it was difficult to differentiate reactive from metastatic LNs with a moderate malignancy rate of 53.5% (23 of 43), and we classified it into highly suspicious malignancy to be on the safe side. The overall malignancy rate of 3 points or more was 86.77%, which was highly suspicious malignancy. Based on the mentioned sonographic features, the operator can choose the appropriate puncture sites during EBUS-TBNA to reduce the number of invalid punctures and to improve diagnostic yield. When the risk-scoring model reveals metastasis, but pathology is negative, repeat EBUS-TBNA or other further surgical procedures are recommended. Notably, EBUS imaging can provide important additional diagnostic information for differentiating metastatic LNs in lung cancer when lesion sampling is inconclusive.

This study still has some limitations. First, the purpose of our study was to predict LN metastasis in patients with suspected lung cancer by using EBUS multimodal imaging. Only reactive LNs from patients with nonspecific intrathoracic lymphadenitis were included in this study, because they were more common in lung cancer patients

than other benign nodes (eg, tuberculosis, sarcoidosis). Using our risk-scoring model for stages of lung cancer would be different from the actuality. Therefore, our risk-scoring model was more suitable for differentiating benign and malignant LNs rather than stages of lung cancer. Second, this study was a single-center retrospective study. Although our risk-scoring model had good discrimination and stability in bootstrap validation, a validation cohort from multicenter prospective trials is recommended to confirm its utility. Third, detection bias was inevitable because of the subjective interpretation of the EBUS results. To decrease the risk of bias, all raters were blinded to the final diagnosis of each LN and the clinical data of patients. On the other hand, we obtained good results of intraobserver and interobserver agreement by using the Cohen κ method.

In conclusion, our newly established risk-scoring model based on EBUS multimodal imaging can effectively evaluate metastatic LNs in lung cancer patients. Incorporating the risk-scoring model into EBUS imaging interpretation workflows may help clinicians to select an appropriate management approach for individual patients.

Source of Funding

This study is supported by Shanghai Chest Hospital Project of Collaborative Innovation (YJXT20190205).

Data Availability Statement

The data presented in this study are stored in our institutional repository and will be shared upon request from the corresponding author.

Conflicts of Interest

Jiayuan Sun is an Editorial Board Member of the journal. This article was subject to the journal's standard procedures, with peer review handled independently of the editor and his research group.

Author Contributions

J.S. designed research; L.W., J.C., and Z.H. conducted research; Z.H. analyzed data; L.W. and Z.H. wrote the manuscript. J.S. had primary responsibility for final content. All authors read and approved the final manuscript. Z.H. and L.W. contributed equally to this work.

REFERENCES

1. Siegel RL, Miller KD, Fuchs HE, Jemal A. Cancer statistics, 2022. *CA Cancer J Clin* 2022;72:7–33.
2. Hirsch FR, Scagliotti GV, Mulshine JL, et al. Lung cancer: current therapies and new targeted treatments. *Lancet* 2017;389:299–311.
3. Silvestri GA, Gonzalez AV, Jantz MA, et al. Methods for staging non-small cell lung cancer: diagnosis and management of lung cancer, 3rd ed: American College of Chest Physicians evidence-based clinical practice guidelines. *Chest* 2013;143:e211S–e250S.
4. Wang Y, Hou K, Jin Y, et al. Lung adenocarcinoma-specific three-integrin signature contributes to poor outcomes by metastasis and immune escape pathways. *J Transl Int Med* 2021;9(4):249–263.
5. Vilmann P, Clementsen PF, Colella S, et al. Combined endobronchial and esophageal endosonography for the diagnosis and staging of lung cancer: European Society of Gastrointestinal Endoscopy (ESGE) guideline, in cooperation with the European Respiratory Society (ERS) and the European Society of Thoracic Surgeons (ESTS). *Endoscopy* 2015;47:c1.
6. Detterbeck FC, Jantz MA, Wallace M, Vansteenkiste J, Silvestri GA, American College of Chest Physicians. Invasive mediastinal staging of lung cancer: ACCP evidence-based clinical practice guidelines (2nd edition). *Chest* 2007;132:202S–220S.
7. Tian Q, Chen LA, Wang RT, Yang Z, An Y. The reasons of false negative results of endobronchial ultrasound–guided transbronchial needle aspiration in

- the diagnosis of intrapulmonary and mediastinal malignancy. *Thorac Cancer* 2013;4:186–190.
8. Li J, Zhi X, Chen J, et al. Deep learning with convex probe endobronchial ultrasound multimodal imaging: a validated tool for automated intrathoracic lymph nodes diagnosis. *Endosc Ultrasound* 2021;10(5):361–371.
 9. Agrawal SP, Ish P, Goel AD, et al. Diagnostic utility of endobronchial ultrasound features in differentiating malignant and benign lymph nodes. *Monaldi Arch Chest Dis* 2018;88:928.
 10. Joseph T, Reddy S, Gupta N, et al. Correlating ultrasonographic features of lymph nodes during endobronchial ultrasound with final outcome. *Cureus* 2022;14:e26554.
 11. Cui XW, Hocke M, Jenssen C, et al. Conventional ultrasound for lymph node evaluation, update 2013. *Z Gastroenterol* 2014;52:212–221.
 12. Fujiwara T, Yasufuku K, Nakajima T, et al. The utility of sonographic features during endobronchial ultrasound-guided transbronchial needle aspiration for lymph node staging in patients with lung cancer: a standard endobronchial ultrasound image classification system. *Chest* 2010;138:641–647.
 13. Evison M, Morris J, Martin J, et al. Nodal staging in lung cancer: a risk stratification model for lymph nodes classified as negative by EBUS-TBNA. *J Thorac Oncol* 2015;10:126–133.
 14. Wang L, Wu W, Hu Y, et al. Sonographic features of endobronchial ultrasonography predict intrathoracic lymph node metastasis in lung cancer patients. *Ann Thorac Surg* 2015;100:1203–1209.
 15. Sun J, Zheng X, Mao X, et al. Endobronchial ultrasound elastography for evaluation of intrathoracic lymph nodes: a pilot study. *Respiration* 2017;93:327–338.
 16. Izumo T, Sasada S, Chavez C, Matsumoto Y, Tsuchida T. Endobronchial ultrasound elastography in the diagnosis of mediastinal and hilar lymph nodes. *Jpn J Clin Oncol* 2014;44:956–962.
 17. Goldstraw P, Chansky K, Crowley J, et al. The IASLC lung cancer staging project: proposals for revision of the TNM stage groupings in the forthcoming (eighth) edition of the TNM classification for lung cancer. *J Thorac Oncol* 2016;11:39–51.
 18. Christiansen IS, Bodtger U, Naur TMH, et al. EUS-B-FNA for diagnosing liver and celiac metastases in lung cancer patients. *Respiration* 2019;98:428–433.
 19. Zhi X, Sun X, Chen J, et al. Combination of ¹⁸F-FDG PET/CT and convex probe endobronchial ultrasound elastography for intrathoracic malignant and benign lymph nodes prediction. *Front Oncol* 2022;12:908265.
 20. Zhi X, Chen J, Wang L, et al. Endobronchial ultrasound multimodal imaging for the diagnosis of intrathoracic lymph nodes. *Respiration* 2021;100:898–908.
 21. Zhi X, Chen J, Xie F, Sun J, Herth FJF. Diagnostic value of endobronchial ultrasound image features: a specialized review. *Endosc Ultrasound* 2021;10:3–18.
 22. Kundel HL, Polansky M. Measurement of observer agreement. *Radiology* 2003;228:303–308.
 23. Sullivan LM, Massaro JM, D'Agostino RB Sr. Presentation of multivariate data for clinical use: The Framingham Study risk score functions. *Stat Med* 2004;23:1631–1660.
 24. Xu T, Chen K, Li G. The more data, the better? Demystifying deletion-based methods in linear regression with missing data. *Stat Interface* 2022;15:515–526.
 25. Steyerberg EW, Vergouwe Y. Towards better clinical prediction models: seven steps for development and an ABCD for validation. *Eur Heart J* 2014;35:1925–931.
 26. Delage A, Beaudoin S. Technical aspects of endobronchial ultrasound-guided transbronchial needle aspiration. *Chest* 2016;150:255.
 27. Hylton DA, Turner S, Kidane B, et al. The Canada Lymph Node Score for prediction of malignancy in mediastinal lymph nodes during endobronchial ultrasound. *J Thorac Cardiovasc Surg* 2020;159:2499–2507.e3.
 28. Ahuja A, Ying M. Sonography of neck lymph nodes. Part II: abnormal lymph nodes. *Clin Radiol* 2003;58:359–366.
 29. Agrawal S, Goel AD, Gupta N, Lohiya A, Gonuguntla HK. Diagnostic utility of endobronchial ultrasound (EBUS) features in differentiating malignant and benign lymph nodes—a systematic review and meta-analysis. *Respir Med* 2020;171:106097.
 30. Wang L, Wu W, Teng J, Zhong R, Han B, Sun J. Sonographic features of endobronchial ultrasound in differentiation of benign lymph nodes. *Ultrasound Med Biol* 2016;42:2785–2793.
 31. Lin CK, Chang LY, Yu KL, Wen YF, Fan HJ, Ho CC. Differentiating metastatic lymph nodes in lung cancer patients based on endobronchial ultrasonography features. *Med Ultrason* 2018;20:154–158.
 32. Morishita M, Uchimura K, Furuse H, Imabayashi T, Tsuchida T, Matsumoto Y. Predicting malignant lymph nodes using a novel scoring system based on multi-endobronchial ultrasound features. *Cancers (Basel)* 2022;14:5355.
 33. Nakajima T, Inage T, Sata Y, et al. Elastography for predicting and localizing nodal metastases during endobronchial ultrasound. *Respiration* 2015;90:499–506.
 34. Schmid-Bindert G, Jiang H, Kähler G, et al. Predicting malignancy in mediastinal lymph nodes by endobronchial ultrasound: a new ultrasound scoring system. *Respirology* 2012;17:1190–1198.
 35. Nagano H, Takumi K, Nakajo M, et al. Dual-energy CT-derived electron density for diagnosing metastatic mediastinal lymph nodes in non-small cell lung cancer: comparison with conventional CT and FDG PET/CT findings. *AJR Am J Roentgenol* 2022;218:66–74.